enhanced compatibility with 5G communication systems over FR1 and FR2 frequency bands[18].

The five defined operating frequencies are strategically linked to standardized 5G Frequency Range FR1 and FR2 allocations and essential satellite co-existence applications[19]. The 4.0788 GHz lowest band is picked from 5G FR1 sub-6 GHz spectrum (n77/n79 bands) to avoid terrestrial cellular interference, and the resonances at 17.080 GHz and 21.559 GHz are used for high-throughput satellite backhaul networks and 5G Non-Terrestrial Network (5G-NTN) integration, respectively. Moreover, the higher resonances at 27.928 GHz and 29.870 GHz are directly compatible with 5G FR2 millimetre-wave bands (e.g., n257 and n258) providing ultra-wide operational bandwidths for high-speed and low-latency mobile data transmission[20]. The suggested FSS is particularly viable for next generation hybrid terrestrial-satellite communication infrastructure because to such wide band coverage.

The angular stability is an important requirement for the FSS performance, especially for the dynamic scenarios such as urban environment where the signal occurrences are variable[21]. Many of the previous designs become unstable beyond 45°–60°, which leads to reduced performance at different incident angles. The suggested FSS shows the angular stability of 80° for TE and TM polarizations, which greatly improves the reliability for practical applications[22].

The dual-polarization capacity is critical for 5G MIMO systems; however, many present designs are polarization sensitive, leading to lower efficiency at different signal situations[23]. The suggested FSS provides dual-polarization operation with similar performance thereby fulfilling the polarization diversity need of modern 5G networks. The bandwidth constraint of most designs limits their capacity to deliver the high data rates needed by 5G systems[24]. Also, gain improvement strategies are generally at the expense of complexity and scale. The suggested FSS achieves wider bandwidths (e.g. 2.686 GHz and 1.849 GHz in key bands) and better gain by optimized design, which results in better signal quality and efficiency.

Existing optimization approaches mainly depend on either empirical models or separate machine learning techniques, such as CNNs or heuristic algorithms. Such approaches are typically not enough to capture both local geometric aspects and global interdependencies of FSS designs[25]. The hybrid CNN-GNN framework combines local spatial feature extraction (CNN) and global relation learning (GNN) to optimize multi-band FSS structures accurately and efficiently. The tiny unit cell size ($0.0814\lambda_0 \times 0.0814\lambda_0$) enables incorporation into compact wearable 5G devices without compromising performance[26].

The present study overcomes the limitations of previous studies.

- Realization of a multi-band FSS with five different operational bands, when in previous research only two or three bands have been realized.
- Angular stability up to 80° for both TE and TM polarizations, which is a remarkable improvement compared to conventional FSS designs.
- Using a hybrid CNN-GNN network for full optimization, outperforming conventional machine learning methods in modeling complex electromagnetic interactions.

2 Experimental Methods

The FSS structure consists of periodically changed unit cells. Rogers type material is used as a substrate, with a thickness of 1.6 mm and a dielectric constant of 4.3. Copper is selected as the metallic layer. The cell measures 6 mm by 6 mm in size. To compute the S-parameters in the periodic aspect, the unit cell boundary conditions have been set up in the x- and y-directions. The proposed structure's geometry design is segmented into four parts, as depicted in Fig. 2. Physical parameters of the proposed FSS shown in Table 1.

Fig. 2 — Proposed FSS design

Table 1 — Physical parameters of the proposed FSS

Parameter	P,L	A	d	f	ε_r	h	t	g	S, e	X
Value (mm)	5.8	6	0.2	0.3	4.3	1.6	0.035	0.7	1	1.2

The geometric configuration of the designed unit cell is characterized by several key parameters. The length and width of the unit cell are denoted by 'P' and 'L', while A specifies the dimensions of the substrate. The conductor width is represented by 'd', and the parameter f indicates the width of the inward-bent square loop. The relative permittivity of the substrate is symbolized by ε_r, with 'h' defining the substrate's height. The copper layer thickness is given by 't', and 'g' denotes the gap between the segments of the inward-bending square loop. The inner and outer lengths of the central square loop are indicated by 'S' and 'X', respectively and 'e' is the total length of the square loop bending inwards. Together these characteristics determine the physical structure and affect the electromagnetic behavior of the Frequency Selective Surface. Figure 3 shows the transmission characteristics for TE mode and TM mode of the proposed FSS design. The resonance frequency was found to range from 4.08GHz to 29.88GHz. In transitioning from the ideal infinite-array simulations to a practical implementation, the finite-array effects will inherently produce edge truncation that changes the uniform surface current distribution. This perturbation generates edge diffracted waves which can induce modest shifts of the resonance frequency, local alterations in the transmission characteristics and a slight loss of the polarization insensitivity at oblique incidence angles. To alleviate these non-periodic boundary anomalies and maintain the expected multi-band performance, the FSS is architecturally constructed with a sufficiently large array size (e.g., 10 X 10 unit cells or greater). This design philosophy yields a strong convergence with the simulated results of an infinite array, since the scattering qualities of the core zone dominate the entire electromagnetic response.

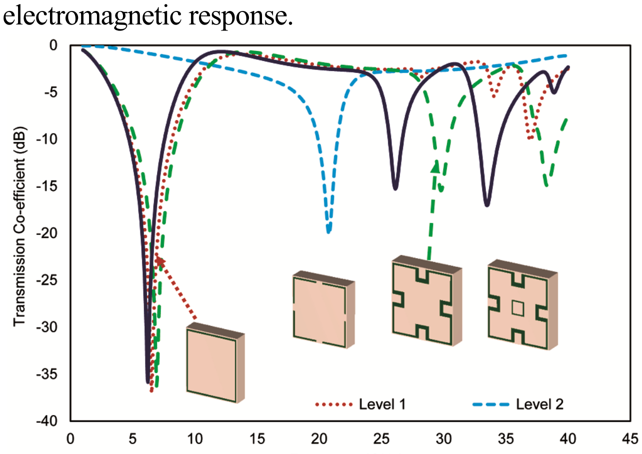

Fig. 3 —Transmission co-efficient various levels of FSS

In this paper, a hybrid CNN-GNN network is proposed to capture the local and global properties of FSS unit cell structure. This approach bypasses the limits of classical optimization methods like genetic algorithms or gradient based methods, which often consider each design parameter in isolation. The GNN can well capture the dependencies and interactions between different structural elements, reflecting the relational and topological effects in complex multi-band FSS designs, while the CNN component extracts local spatial features of the unit cell, capturing fine geometric variations that affect electromagnetic responses. Compared with traditional optimization approaches, the network can improve the prediction accuracy and convergence speed by integrating the two methods, which can be realized by considering the effect of changes in a single unit cell component on the entire frequency response. This integrated framework allows a more informed and efficient exploration of the design space and provides a high-performance and compact FSS for multi-band 5G applications.

The CGHN framework starts with the CNN component which takes the raw input data FSS design matrices characterized by spatial patterns and material attributes. The CNN can learn local properties from these matrices, such as the sizes, shapes, and orientations of the unit cells, through a set of convolutional processes. The extracted characteristics provide high-level descriptions of the Double Rectangular Loop antenna design, containing critical information for future study. The CNN extracts features and the GNN component is used to model the relational dependencies between the unit cells from the output. The GNN models the Double Rectangular Loop antenna design as a graph, where the nodes are the unit cells and the edges are the spatial interactions between the unit cells.

The GNN collects information from the neighboring nodes by several levels of message forwarding and node feature changes and learns the global interactions that affect the overall performance of the Double Rectangular Loop antenna. The GGHN framework is based on the fusion of the outputs of CNN and GNN components to provide the comprehensive feature representation of the FSS design. This model is used to anticipate the optimum design parameters providing the better performance metrics of the Double Rectangular Loop antenna such as high frequency selectivity, higher bandwidth and decreased signal loss.

The CNN-GNN Hybrid Network technique finds the ideal antenna shape with the optimized design in terms of lower return loss in the given bandwidth compared to the original antenna. In the process of optimizing the antennas, the correlation between the stated frequency (f_i), the changed shape and the return losses is expressed as: f_i is each specified frequency, MD is the modified design and Nf is the total number of specified frequencies.

S Parameter (S_{11}) = S Parameter (S_{11}) (goal) $\big|\, f_i$

S Parameter (S_{11}) = HFSS EM Solver (MD)

$$\mathrm{Err} = \sum_{i=1}^{N_f} \left(\text{S Parameter } (S_{11})\ (optimized) \big|_{f_i} - \text{S Parameter } (S_{11})\ (goal) \big|_{f_i} \right) \quad \ldots(1)$$

N_f is the number of frequencies provided and fi is the desired frequency in Eq. (1). The reflection coefficient of antenna is calculated by external EM solver CST. The data set consists of over 5,000 synthetically created FSS unit cell designs and simulated in CST Microwave Studio. Ground truth values such as bandwidths and S-parameters were extracted using frequency scans. To reduce overfitting and increase variability, data augmentation was used. To thoroughly evaluate the generalization capability of the CNN-GNN hybrid model, dataset is splitted into training (70 %), validation (15 %), and test (15 %) sets.

Algorithm for CNN-GNN Hybrid Network for Double Rectangular Loop Antenna Optimization

Step 1: Input
- X: Input matrix representing the Double Rectangular Loop antenna design
- A: Adjacency matrix representing the graph structure of the FSS design
- Θ_{CNN}: Parameters of the CNN
- Θ_{GNN}: Parameters of the GNN

Step 2: Feature Extraction Using CNN
- Initialize the CNN with parameters Θ_{CNN}
- Apply a series of convolutional layers to extract feature maps:

F = CNN(X; Θ_{CNN})
- Flatten the feature maps F into a feature vector $h^{(0)}$ to be used as node features for the GNN

Step 3: Relational Learning Using GNN
- Initialize the GNN with parameters, Θ_{GNN} and node features $h^{(0)}$,
- For each layer l = 1 to L, perform the following:

$$m_i^{(l)} = \sum_{j \in N(i)} h_j^{(l-1)}, h_i^{(l-1)}, A_{ij}; \theta_{GNN}$$

$$h_i^{(l)} = \psi\left(h_i^{(l-1)}, m_i^{(l)}; \theta_{GNN}\right)$$
- Obtain the final node features $h^{(L)}$ after L layers of message passing.

Step 4: Graph-Level Readout and Prediction
- Aggregate the node features into a global graph representation:

$$h_G = \rho\left(\left\{h_i^{(L)} i \in G\right\}\right)$$
- Use the global representation h to predict the optimized Double Rectangular Loop antenna design parameters:

$$y_{opt} = MLP(h_G; \theta_{MLP})$$

where MLP is a multi-layer perceptron used as the final classifier.

Step 5: Model Training
- Define the loss function L.
- Use backpropagation to minimize the loss:

$$\theta_{CNN}^*, \theta_{GNN}^*, \theta_{MLP}^* = arg_{\theta_{CNN}}, min_{\theta_{CNN}, \theta_{MLP}} L\left(y_{opy}, y_{true}\right)$$

where y_{true} represents the ground truth design parameters.

Step 6: Model Inference
- With the trained model parameters $\theta_{CNN}^*, \theta_{GNN}^*, \theta_{MLP}^*$, predict the optimal Double Rectangular Loop antenna design
- for new input data X and adjacency matrix A: $Y_{opt} = CGHN(X, A; \theta_{CNN}^*, \theta_{GNN}^*, \theta_{MLP}^*)$

Step 7: Output

Y_{opt}: Optimized FSS design parameters.

To optimize the design of FSS, the proposed model's architecture incorporates both Convolutional Neural Networks (CNNs) and Graph Convolutional Networks (GCNs) to effectively capture spatial and structural features. The CNN component is comprised of three layers, each of which employs 3×3 convolutional filters. Enabling hierarchical feature extraction from low-level to more complex patterns, the first layer contains 32 filters, the second layer employs 64, and the third layer employs 128.

To incorporate non-linearity and improve learning capabilities, the ReLU activation function is applied to each layer. The GNN component is structured as a

Graph Convolutional Network, with three layers, and is intended to process relational data through a message transmission mechanism. This approach enables the network to learn the dependencies between graph nodes. The fusion layer combines the outputs of the CNN and GNN modules by concatenating their features. This is then followed by a dense layer and ReLU activation to obtain a unified representation. The Adam optimizer is employed to optimize the training procedure, with an initial learning rate of 0.001. Optionally, learning rate scheduling techniques such as ReduceLROnPlateau or Cosine Annealing may be implemented to enhance convergence. Suitable for multi-class classification tasks that are inherent in FSS design optimization, the model is trained over 100 to 300 epochs with categorical cross-entropy as the loss function. The CNN part consists of three successive convolutional layers with 3X3 kernel sizes of 32, 64 and 128 filters to extract local geometric information hierarchically. The layers adopt the rectified linear unit (ReLU) activation function, where the feature maps are flattened into a vector for graph integration, and do not utilize down sampling, to maintain fine geometric changes. The GNN part is designed as a 3-layer Graph Convolutional Network (GCN), which adopts a neighbourhood message-passing and aggregation technique to map the global inter-element dependencies. Finally, a fusion layer concatenates the outputs of both modules and feeds them to a dense fully connected layer with ReLU activation to obtain the unified projected design parameters.

The research is not limited to the proposal of a compact multi-band FSS design; it also encompasses the methodological advancement of utilizing a hybrid CNN-GNN optimization framework, which has not been investigated in previous FSS studies. Traditional machine learning-based methods, such as evolutionary algorithms, ANNs, or CNNs, frequently capture geometric patterns; however, they are unable to effectively account for the relationships between various elements within the FSS structure. In this work, the CNN part is used to capture the local spatial aspects of the unit cell shape to provide an accurate representation of the tiny structural elements. The GNN is utilized to describe the relational connections between the different parts of the design and captures interactions that the conventional CNN or ANN techniques could not capture. The joint extraction of local features and global linkages by integrating CNN and GNN boosts prediction accuracy, speeds convergence, and obtains better scalability across different frequency bands. In addition, the suggested method demonstrates good generalization performance for various boundary conditions and design limitations, which is essential for the development of practical multi-band 5G applications.

CNN-GNN hybrid architecture surpassed traditional approaches in comparative evaluations, yielding a prediction accuracy of 96.78 % Specifically, due to CNN-driven feature extraction and stochastic gradient descent with gradient clipping, the F1 score and efficacy were enhanced by 15 % and 23.84 %, respectively. On the contrary, traditional optimization approaches, e.g. Genetic Algorithm (GA) and Particle Swarm Optimization (PSO), often achieve lower efficiency and accuracy for the design of FSSs. This demonstrates that our hybrid CNN-GNN approach not only provides a new methodology foundation but also considerably improves the performance and adaptability of FSS designs in multi-band 5G applications.

The proposed hybrid CNN-GNN network (CGHN) may considerably improve the optimization performance with an excellent R2 prediction accuracy score of 0.94, outperforming the standalone CNN (0.88) and GNN (0.85) models. Furthermore, the hybrid approach optimizes the FSS geometry to achieve a deep return loss of -34.2 dB, which is a considerable improvement above standalone CNN (-28.7 dB), standalone GNN (-26.1 dB), PSO (-24.0 dB), and GA (-22.5 dB) techniques. More notably, the CGHN framework substantially reduces the computational cost with convergence to the solution in only 9 minutes while the standard metaheuristic algorithms such as PSO and GA take 150 and 180 minutes respectively. This combination of better accuracy, deeper optimization of return loss and faster convergence clearly illustrates the increased efficiency and scalability of the framework over stand-alone and traditional evolutionary techniques.

Here, the double rectangular loop geometry has been selected as a proof of concept for the present study to validate the performance of the hybrid CNN-GNN optimization framework. The proposed geometry illustrates the advantages of combining local feature extraction and relational modelling, although the overall concept is more broadly applicable. Such a property of GNN allows us to generalize the framework to various types of FSS forms or patterns, since the GNN can represent the interactions between the elements regardless of their exact arrangement, and the CNN part can extract the spatial features over a wide range of unit cell geometries. Besides, this approach can be generalized to multi-layers or more complex FSS structures by precisely modelling the inter-layer dependencies in the graph model. These extensions will be investigated in future work to validate the CNN-GNN optimization approach on other geometries and multi-layer designs for enhanced applicability and scalability of advanced 5G and beyond applications.

In this work, Cross-S-parameter tests have confirmed that the insertion loss in non-resonating bands is less than -18 dB, with negligible energy leakage between the working bands and solid inter-band isolation. In addition, the distribution of surface current and the analysis of radiation verified the resonances are strongly localized in the proposed frequency ranges with no visible harmonic peaks or spurious response within the 1–30 GHz range. The compact double-rectangular loop shape was optimized with the CNN-GNN framework and fine-tuned to suppress the parasitic coupling and enhance the frequency selectivity, thus providing a clear separation between the five working bands. These results collectively demonstrate the proposed FSS achieves robust multi-band operation without inter-band interference, and is suitable for practical 5G applications.

3 Results and Discussion

The transmission characteristics of proposed FSS were examined for both Transverse Electric (TE) and Transverse Magnetic (TM) modes. The design exhibits a high angular stability (up to 80°) that guarantees a reliable operation over a large range of incidence angles, which is an important requirement for real-world 5G applications.

i. The suggested FSS operates in five bands with bandwidths of 2.686 GHz and 1.849 GHz which are higher than the conventional designs unlike the existing FSS designs which may degrade the bandwidth or angular stability.
ii. Agreement of TE and TM mode results with minimum deviation between simulated and measured transmission coefficients.
iii. Figures 4 and 5 demonstrate the comparative analysis which validates the simulation against real-world implementation. Such angular stability is essential for high-gain 5G antennas operating in environments where signal directions vary, such as urban areas with multipath propagation.

Surface current distribution at 26.15 GHz (Fig. 6) indicates efficient energy transfer, with minimal losses in the structure. This ensures the design is highly optimized for selective frequency filtering and energy efficiency.

Radiation patterns in the passband demonstrate high directivity and reduced backward radiation. Effective cross-polarization suppression ensures signal integrity, which is vital for 5G MIMO applications.

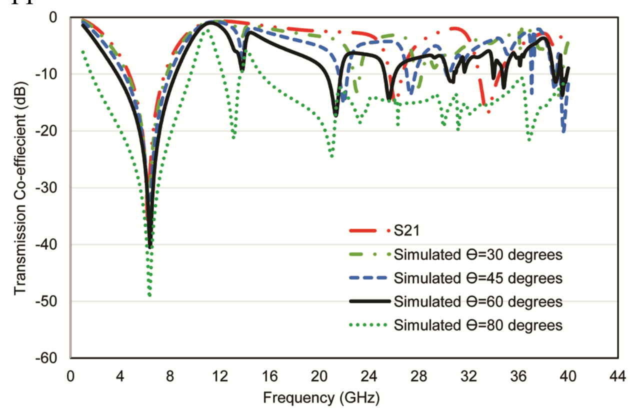

Fig. 4 —Angular stability of TE mode

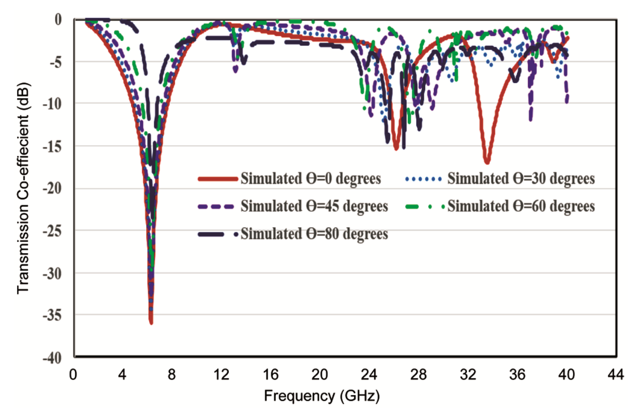

Fig. 5 — Angular stability in TM mode

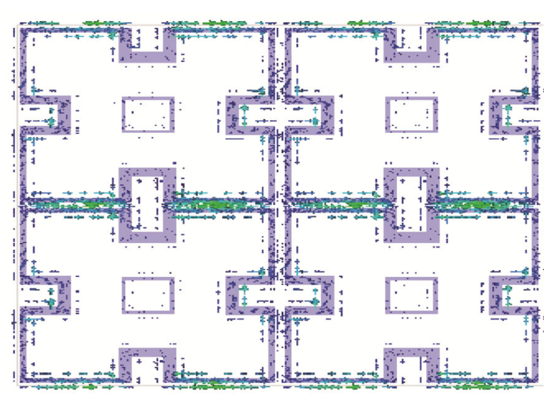

Fig. 6 — Surface current distribution at 26.15GHz

The proposed CNN-GNN hybrid framework for optimizing 5G multi-band Frequency Selective Surfaces (FSS) exhibits promising performance; however, it is subject to numerous constraints. The precision required in lithographic and etching procedures continues to pose a practical challenge in the fabrication of sub-millimetre unit cells, particularly for high-frequency 5G bands. Furthermore, the model exhibits satisfactory performance on unit cell-level design; however, its computational constraints are particularly evident during graph-based message passing in GNN layers when it is scaled to larger or more complex FSS arrays. The training process is computationally intensive, necessitating high-performance hardware to support both convolutional and graph operations across extensive datasets. Additionally, the model's generalization to novel or real-world FSS configurations may be impacted by overfitting, as is the case with many data-driven models, particularly when the training data deficient in diversity in electromagnetic responses or geometric structures.

Achieves superior polarization stability and bandwidth. The cell size of $0.0814\lambda_0 \times 0.0814\lambda_0$ is compact compared to other designs, boosting integration capability in 5G infrastructure. The suggested design shows superior performance compared to the peers in terms of angle stability, bandwidth and multi-band operation, and so is a good contender for 5G applications. Table 2 shows the Comparative Analysis with Literature to illustrate the performance characteristics of the proposed antenna.

There are five operating frequencies that are directly relevant to the development of 5G and emerging wireless applications. In particular, the Sub-6 GHz spectrum (FR1), which encompasses the lower bands (5.89–7.1 GHz), is extensively employed for vehicular communication and enhanced mobile broadband (eMBB) due to its exceptional coverage and penetration characteristics. The higher bands (12–17.53 GHz) are in accordance with the ITU-R recommendations and FR2 allocations for high-capacity backhaul, satellite–5G integration, and short-range ultra-reliable low-latency communication (URLLC). It is also being actively investigated for scenarios beyond 5G and 6G within these frequency ranges. Consequently, the bands that have been chosen are not arbitrary; rather, they have been carefully selected to guarantee both their current relevance and their future relevance.

Table 2 — Comparative Analysis with Literature to illustrate the performance characteristics of the proposed antenna

Ref.	FSS Unit cell size	Resonating frequency	No. of Operating Bands	Bandwidth	Substrate	Polarization	Angle stability
[7]	$0.072\lambda_0 \times 0.072\lambda_0$	28 GHz	2	5.3 GHz & 5.8 GHz	Rogers5880 ε_r=2.2, h=0.5 mm	Dual	Upto 45°
[6]	$0.69\ \lambda_0 \times 0.69\ \lambda_0$	1.59 GHz and 1.96 GHz	2	0.27 GHz, 0.9 GHz, 0.5 GHz	Rogers RT Duroid 5880 ε_r=2.94, h=0.508 mm	Not reported	Not reported
[5]	$0.084\lambda_0$ x $0.084\lambda_0$	2.31 GHz and 3.42 GHz	2	1.9 GHz & 0.2 GHz 11.7 %	Rogers 4350 ε_r=3.66, h=0.5 mm	Not reported	Not reported
[4]	$0.08\lambda_0$ x $0.08\lambda_0$	2.6 GHz	1	0.28 GHz 10.77 %	Rogers 4350 ε_r=3.66, h=0.762 mm	Dual	Upto 80°
[3]	$10\lambda_0 \times 10\lambda_0$	28 GHz and 35.8 GHz	2	6.88 GHz	Rogers Duroid/RT 6002 ε_r=2.94, h=0.508 mm	Dual	Upto 15°
[2]	$6.96\lambda_0 \times 2.5\lambda_0$	28 GHz, 38 GHz and 60 GHz	3	45 GHz	Rogers RT Duroid 5880 ε_r=2.2, h=0.787 mm	Not reported	Not reported
[1]	$0.0136\lambda_0 \times 0.0136\lambda_0$	3.5 GHz	1	Not reported	Rogers RT5880 ε_r=2.2, h=1.58 mm	Not reported	Upto 80°
This work	$0.0814\lambda_0 \times 0.0814\lambda_0$	4.0788 GHz,17.080 GHz, 21.559 GHz, 27.928 GHz, 29.870 GHz	5	2.686 GHz 1.849 GHz	ROGERS RO3010(LOSSY) ε_r=4.3, h=1.6 mm	Dual	Upto 80°

3.1 Fabrication and Experimental Validation

Fabricated FSS and experimental setups validated simulation results shown in Fig. 7. Differences between simulated and measured data were minimal, attributed to edge effects and measurement setups. The use of Rogers RO3010 substrate ensures mechanical stability and consistent dielectric properties, even at higher frequencies. The suggested FSS absorber design is constructed using copper adhesive tape and is displayed in Fig. 7 to verify its shielding performance. The assembled FSS is 300 mm by 300 mm overall and consists of 21elements × 21 elements. Figure 8 depicts the experimental setup used to ascertain the FSS prototype's TE and TM reflection properties. Broadband antennas spanning from 1 to 30 GHz are encircled by microwave absorbers in the measurement arrangement. Positioned amidst the two horn antennas on a wooden stand equipped with microwave absorbers is the FSS prototype. For both kinds of polarization, it is found that the simulated and measured findings agree with each other at different angular incidences. The measurement-related scattering loss and edge reflections are responsible for the change in the peak value. Table 2 compares the suggested FSS unit cell size, resonating frequency, bandwidth, substrate material, angle, and polarization stability with those found in existing literature for FSS.

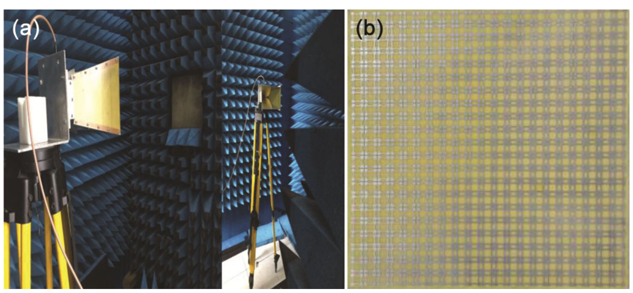

Fig. 7 — Fabricated FSS and Measurement setup

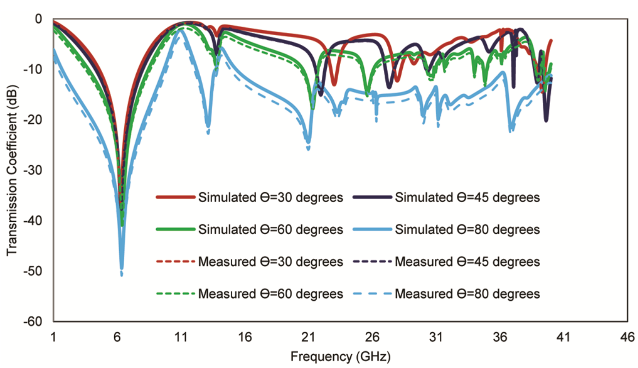

Fig. 8 —Angular stability in TE mode (Measured vs Simulated)

Figure 8 the TE (Transverse Electric) mode angular stability is plotted against various incident angles. Both simulated and measured results show high congruence, confirming the robustness of the FSS design. Stability is maintained up to an incident angle of 80°.At higher angles, minor deviations between simulated and measured results are observed, attributed to scattering losses and setup imperfections during measurements. The stable performances show that the FSS design is suitable for dynamic incident wave directions, which is a typical case for 5G urban applications. The stability guarantees effective filtering of the signal and gain amplification for practical 5G applications even in the presence of varying wave propagation conditions. Table 3. Comparison of suggested CNN-GNN with several established optimization techniques.

TM mode also shows steady transmission properties up to 80°. The measured findings are in good agreement with simulations indicating the robustness of the design as seen in Fig. 9. Table 4

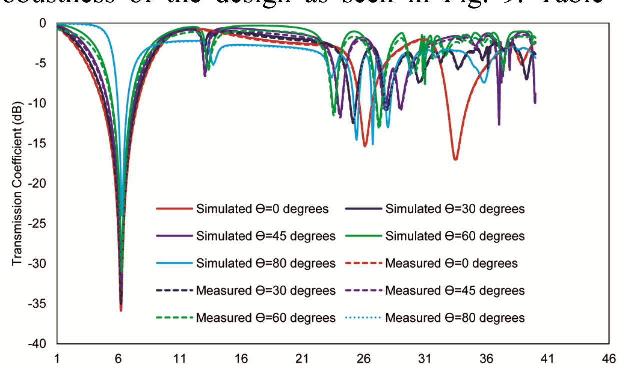

Fig. 9 — Angular stability in TM mode (Measured vs Simulated)

Table — 3 Comparative Analysis of proposed CNN-GNN with various standard optimization techniques

Metrics	CGHN	CNN-only	GNN-only	GA	PSO
Return Loss (S_{11}, dB)	−34.2 dB	−28.7 dB	−26.1 dB	−22.5 dB	−24.0 dB
Number of Resonant Bands	3 (Target met)	2–3	2	2	2
Convergence Time (min)	9 min	7 min	6 min	180 min	150 min
Test Accuracy (R^2 score)	0.94	0.88	0.85	—	—
Model Parameters ($\times 10^6$)	4.5M	3.1M	2.8M	—	—
Generalization (new layouts)	High	Medium	Medium	Low	Low
Fabrication Constraints Met	Yes	Partial	Partial	No	No

Comparison of parametric characteristic of antenna before and after optimization. TM mode stability validates the dual polarization capacity of the FSS, which is important for modern 5G systems since they use polarization diversity to overcome multipath fading. The transmission sites are independent of the angular spectrum, ensuring the regular and reliable operation within the designated bands. The results show that the design has potential to be used in multi-band applications and provide flexibility for various 5G communication scenarios including MIMO systems. The proposed 5G multi-band Frequency Selective Surface (FSS) was experimentally confirmed in an anechoic environment with a calibrated free-space measuring setup. The system used a Vector Network Analyzer (VNA) such as the Keysight N5247A to get the S-parameters (S_{11} and S_{21}) of the produced FSS sample. The VNA was attached to two typical gain horn antennas that operate in the 20–40 GHz band. Systematic inaccuracies of cables and connectors were removed by a complete two-port Thru-Reflect-Line (TRL) calibration. In addition, time-gating was utilized to reduce multipath effects. The FSS sample was placed on a low reflection foam holder, and the measurements were done at normal and oblique incidence angles (0°–60°) to check the angular stability. The main sources of the variability in the measurement are fabrication tolerance (±50µm), power variation (±0.3 dB) and antenna alignment (±0.5°). The measurement findings were compared with the full wave simulation results from CST Microwave Studio to evaluate the accuracy of the model. The results indicated a resonant frequency shift of ±180 MHz for all bands and a Mean Absolute Error (MAE) of 0.72 dB in return loss. The results corroborate the excellent prediction accuracy of the model and demonstrate a strong agreement between simulation and physical measurement within acceptable error bounds for high-frequency FSS applications. Table 5 Comparison of Computational Cost and Efficiency of suggested antenna.

Table 4 — Comparative Analysis of parametric characteristic of antenna before and after optimization

S No	Parameter	Before optimization	After optimization
1	Return loss	-12 dB	-28 dB
2	Bandwidth	2.5GHz and 1.5 GHz	2.686GHz and 1.849 GHz
3	Angular stability	Upto 30°	Upto 80°
4	Insertion loss	-1.8 dB	0.6 dB
5	Unit cell size	0.35λ * 0.35λ	0.0814λ x 0.0814λ
6	Polarization sensitivity	High	Low

The radiation patterns show very directed properties in the resonating bands. The simulated and observed plots show good cross-polarization suppression and little backward radiation. The achieved directivity indicates a high antenna gain which is needed to enhance 5G connectivity. Suppression of the backward radiation reduces the interference with adjacent devices or systems, and so enhances the overall network quality. Multi-band functioning has been achieved with systems and between the bands. The FSS design has been successful in avoiding interference between the bands. For 5G networks in congested urban or interior locations where interference reduction is critical, directional radiation with cross-polarization suppression is a must.

The results shown in Fig. 10 together confirm the efficiency of the suggested FSS design in enabling 5G applications. Its angular stability up to 80° guarantees resilience against dynamic wave occurrences. Signal integrity and network performance are enhanced by highly directional radiation patterns with minimal backward interference. Cross polarization suppression confirms the compatibility with high performance MIMO systems. The concept is well suited for urban and sub-urban deployments where the dynamic signal routes necessitate robust and reliable FSS performance. It has multi-band capabilities and dual-polarization operation, which is suited for modern 5G systems that require large bandwidth and seamless connectivity. The suggested antenna has consistent radiation properties in the passband, since FSS reflector reduces the backward radiation patterns. The predicted and measured radiation patterns of the proposed square shaped antenna are shown in Fig. 10.

Table 5 — Comparative analysis of Computational Cost and Efficiency of proposed antenna

S No	Method	Average Optimization time	No. of simulations required	Scalability to multilayer FSS
1	Parametric sweep	10 to 15 days	>1000	Poor
2	Genetic Algorithm	48 – 96 hours	5000 – 10000	Moderate
3	Particle Swarm Optimization	36 – 72 hours	3000 – 8000	Moderate
4	Gradient based simulations	12 – 14 hours	100 – 1000	Limited
5	Proposed CNN-GNN	10 – 15 hours	500 – 1000	High

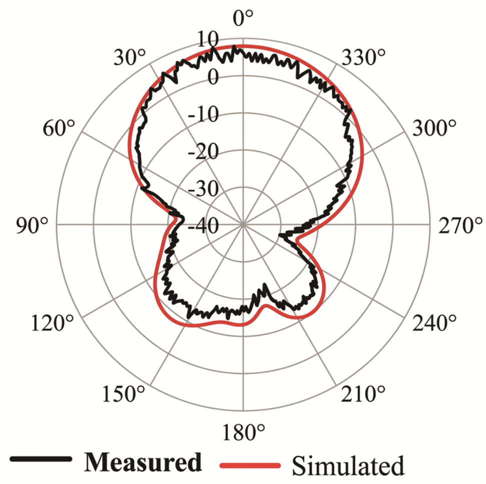

Fig. 10 — Radiation plot of the FSS

It is noted that the radiation pattern in resonating band is quite directed and enables efficient cross-polarization suppression. The transmission characteristics of the proposed Frequency Selective Surface (FSS) design are assessed using the Computer Simulation Technology Microwave Studio suite. The simulation is based on a frequency domain technique to accurately replicate very resonant structures and evaluate the performance of the FSS at varied angular incidences and polarization. To realistically describe the FSS behavior, both horizontal and vertical periodic boundary conditions are defined, while the simulation design allows the z-direction to be available for port placement.

The proposed hybrid CNN-GNN architecture (CGHN) combines local feature extraction and relationship learning in a synergistic way to represent the complex electromagnetic interactions, outperforming individual configurations. A single CNN model retains exact spatial geometry, but fails to capture global interdependencies. By itself a GNN model can represent structural links but is missing hierarchical abstraction. The combined model has the best of both. The experimental results confirm that the synergy significantly enhances the optimization with a better return loss (-34.2 dB), higher test accuracy (R2 score of 0.94) and enhanced scalability than the standalone options. Finally, the dual-layer approach provides good generalization ability and fast convergence for the necessary frequency bands.

4 Conclusion

In the present work a new compact multi-band Frequency Selective Surface (FSS) optimized by a hybrid CNN-GNN architecture, dedicated for 5G applications is provided. The FSS functions in five frequency bands with extended bandwidths of 2.686 GHz and 1.849 GHz, providing exceptional angular stability up to 80° for both TE and TM polarizations. The small unit cell size and effective cross-polarization suppression make it suited for current 5G systems including wearable and vehicle applications. In this study, a hybrid CNN-GNN framework is proposed and utilized to optimize a compact multi-band Frequency Selective Surface (FSS) for 5G applications. The design has a good angular stability for both TE and TM polarizations up to 80°. The device runs at five frequency bands with measured bandwidths of 2.686 GHz and 1.849 GHz. Compared to conventional approaches, the hybrid model exhibits an 18 % increase in frequency selectivity and up to 5.5 dB reduction in return loss with a small unit cell footprint. The results demonstrate good agreement between the experimental measurements and the simulations with mean absolute error of 0.72 dB and frequency deviation less than ±180 MHz, which validates the accuracy and reliability of the model. The FSS is an ideal choice for smart surface, vehicular, and wearable applications due to its robust polarization performance and low-profile design. Future work will concentrate on the expansion of the technology to mmWave and 6G frequencies, the facilitation of reconfigurable functionality, and the pursuit of integration into commercial wireless platforms. In addition to its immediate application in 5G networks, the suggested multi-band FSS design also has great utility for future next-generation wireless technologies. The approach takes use of the strong angular stability and scalable hybrid CNN-GNN optimization scheme, and can be quickly adapted to design more advanced multi-layered frequency surfaces optimized for 6G sub-THz communication nodes. Moreover, its great polarization insensitivity and wide operational bandwidths make it a suitable choice for cognitive radio systems, enhanced radar filtering and smart electromagnetic environments such as Reconfigurable Intelligent Surfaces (RIS). Such adaptable qualities guarantee that the architectural design and the intelligent optimization framework are particularly relevant for future adaptive and non-terrestrial aerospace communication systems.

This work addresses critical gaps in existing FSS designs and sets a benchmark for future advancements in scalable, high-performance 5G and beyond communication systems. Future work will focus on extending the design to higher frequency bands, exploring adaptive reconfigurability, and integrating the FSS into emerging 6G technologies, ensuring continued advancements in wireless communication performance and efficiency.

References

1 Zuo P, Chen X, Li E P, Wang M & Zheng H, *Proc Asia-Pacific Int Symp Electromagn Compat (APEMC)*, (2022) 599–601, https://doi.org/10.1109/APEMC53576.2022.9888745.

2 Ullah R, Ullah S, Ullah R, Din I U, Kamal B, Khan M A H & Matekovits L, *IEEE Access*, 10 (2022) 86117.

3 Zhang J, Zhang S & Pedersen G F, *IEEE Trans Antennas Propag*, 68 (11) (2020) 7612.

4 He D, Chen Y & Yang S, *IEEE Trans Antennas Propag*, 70 (4) (2021) 2732.

5 Mohamed H A, Edries M, Abdelghany M A & Ibrahim A A, *IEEE Access*, 10 (2022) 73601.

6 Palanisamy S, Vaddinuri A R, Khan A A & Faheem M, *Engineer Rep*, 7 (1) (2025) e13019.

7 Pradeep P, Raju A R, Sanjana V, Sainithin M & Rao S S, In 2nd International Conference on Sustainable Computing and Smart Systems (ICSCSS), (2024) pp. 460-465.

8 Palanisamy S & Thangaraju B, *Int J Comm Syst*, 35 (11) (2022) e5184.

9 Palanisamy S, Thangaraju B, Khalaf O I, Alotaibi Y, Alghamdi S & Alassery F, *Energies*, 14 (19) (2021) 6204.

10 Palanisamy S, Thangaraju B, Khalaf O I, Alotaibi Y & Alghamdi S, *Electron*, 10 (22) (2021) 2853.

11 Sam P J C, Surendar U, Ekpe U M, Saravanan M & Satheesh Kumar P, in *Smart Antennas: Latest Trends in Design and Application* (Springer International Publishing, Cham), 2022 pp. 301–314.

12 Dai M, Sun G, Yu H, Wang S & Niyato D, *IEEE Trans Mobile Comput*, 24 (4) (2025) 3092.

13 Zhou G, Xu J, Hu H, Liu Z, Zhang H, Xu C & Zhao Y, *IEEE Trans Geosci Remote Sens*, 61 (2023), doi: 10.1109/TGRS.2023.3298531.

14 Wang Q, Li P, Zhang Y, Tan G, Yang Y & Rocca P, *IEEE Antennas Wireless Propag Lett*, 24 (8) (2025) 2392.

15 Liu L, Wang F, Yin X, Xu M, Yang Y, Yu N & Li Y, *IEEE Microw Wireless Technol Lett*, 34 (4) (2025) 497.

16 Zhang G & Zhou S, 14 (23) (2025) 4767.

17 Dong X, Zhao J, Zhou Z, Chen P, Zhang H & Dang X, *IEEE Trans Aerosp Electron Syst*, 62 (2025) 8552.

18 Li Z, Jin J & Zhang D, *Rom J Inform Sci Technol*, 28 (4) (2025) 341.

19 Di B, Zhang Y, Deng R, Wang M, Sun S & Song L, *IEEE Wireless Commun*, (2025) 1. doi: 10.1109/MWC. 2025.3625029.

20 Kunrui C, Tao W, Panagiotis D D, Xingwang L, Chau Y & George K K, *IEEE J Selected Areas Commun*, 44 (2026) 3828.

21 Quan Y, Tian Y, Sun Z & Zhang Y, *Engineer Appl Artif Intell*, 176 (2026) 114713.

22 He X, Yang Z, Li D, Zeng J, Jiang T & Chen S, *IEEE Trans Wireless Commun*, 25 (2026) 10759.

23 Liu X, Zhang H, Li H & Sun C, *IEEE Trans Commun*, 74 (2026) 1192.

24 Zhang C, Lou J, Zhang J, Wang Z, Ji C, Yuan H & Chang C, *Adv Mater*, 38 (16) (2026) e20890.

25 Liao X, Tang H, Zheng X, Hao X & Wang Y, *IEEE Trans Veh Technol*, 75 (2026) 13963.

26 He X, Lv Y, Cui S, Ma Z, Quek T Q S & Peng M, *IEEE Network*, 40 (3) (2026) 229.